Quantitative Spatially Resolved Measurements of Mass Transfer Through Laryngeal Cartilage

Julie V. Macpherson,* Danny O'Hare,# Patrick R. Unwin,* and C. Peter Winlove§
*Department of Chemistry, University of Warwick, Coventry CV4 7AL, #Department of Pharmacy, University of Brighton, Brighton BN2 4GJ, and §Physiological Flow Studies Group, Imperial College of Science Technology and Medicine, London SW7 2BZ, United Kingdom

ABSTRACT The scanning electrochemical microscope (SECM) is a scanned probe microscope that uses the response of a mobile ultramicroelectrode (UME) tip to determine the reactivity, topography, and mass transport characteristics of interfaces with high spatial resolution. SECM strategies for measuring the rates of solute diffusion and convection through samples of cartilage, using amperometric UMEs, are outlined. The methods are used to determine the diffusion coefficients of oxygen and ruthenium(III) hexamine [$Ru(NH_3)_6^{3+}$] in laryngeal cartilage. The diffusion coefficient of oxygen in cartilage is found to be ~50% of that in aqueous electrolyte solution, assuming a partition coefficient of unity for oxygen between cartilage and aqueous solution. In contrast, diffusion of $Ru(NH_3)_6^{3+}$ within the cartilage sample cannot be detected on the SECM timescale, suggesting a diffusion coefficient at least two orders of magnitude lower than that in solution, given a measured partition coefficient for $Ru(NH_3)_6^{3+}$ between cartilage and aqueous solution, $K_p = [Ru(NH_3)_6^{3+}]_{cartilage}/[Ru(NH_3)_6^{3+}]_{solution} = 3.4 \pm 0.1$. Rates of $Ru(NH_3)_6^{3+}$ osmotically driven convective transport across cartilage samples are imaged at high spatial resolution by monitoring the current response of a scanning UME, with an osmotic pressure of ~0.75 atm across the slice. A model is outlined that enables the current response to be related to the local flux. By determining the topography of the sample from the current response with no applied osmotic pressure, local transport rates can be correlated with topographical features of the sample surface, at much higher spatial resolution than has previously been achieved.

INTRODUCTION

Cartilage is a dense, avascular, connective tissue which acts as a load-bearing material. It consists of an extensive extracellular matrix (ECM), which contains a variety of negatively charged proteoglycan macromolecules, cells, and interstitial fluid embedded in a network of collagen fibers. Knowledge of the rate and mechanism of water and solute transport through the ECM is important in several contexts. First, the rate at which water is redistributed under the influence of applied loads is the principal determinant of the viscoelastic properties of the tissue (Mow et al., 1984). Second, the normal physiological functioning of the tissue is maintained by the convective-diffusive transport of nutrients, metabolites, and signal molecules between the chondrocytes and synovial fluid (Urban, 1990). Although it is frequently hypothesized that disturbances in mass transport are either a cause or a consequence of the major changes in the biochemical composition of cartilage, during degenerative diseases such as osteoarthritis and rheumatoid arthritis, traditional experimental methodologies for investigating transport processes provide insufficient spatial resolution to test these hypotheses.

Hitherto, the overwhelming majority of studies of water and solute transport in cartilage have measured the bulk characteristics, averaged over macroscopic volumes of tissue. Steady-state characteristics have predominantly been determined using two-compartment diffusion cells (Maroudas, 1968, 1970), while several types of desorption methods have been used to determine transient diffusion characteristics across thin slices and intact plugs of articular cartilage (Allhands et al., 1984; Torzilli et al., 1987). The latter technique has provided most spatially resolved information on transport. By assaying sections of tissue cut parallel to the articular surface, variations in solute distribution and diffusion through the thickness of the cartilage could be determined with a resolution of ~100 μm, but the data were averaged across the plug, which was typically several millimeters in diameter.

Ultrastructural studies with transmission electron microscopy (Bloebaum and Wilson, 1980) and atomic force microscopy (Jurvelin et al., 1996) have revealed that the 3-D structure of cartilage is heterogeneous at the microscopic level. Clearly, in order to provide a detailed understanding of the relationship between structure and permeability, techniques are required that can determine the mass transport characteristics of the tissue, with a spatial resolution approaching that of the topographical imaging techniques currently available. Although the recent introduction of nuclear magnetic resonance spectroscopy and imaging (Burstein et al., 1993; Fischer et al., 1995) has partly addressed the problem for intact cartilage samples, the best spatial resolution attainable with this technique is currently ~200 μm.

The goal of this paper is to demonstrate that many of the above limitations may be overcome through the use of the scanning electrochemical microscope (SECM) (Bard et al., 1989, 1991, 1993; Macpherson and Unwin, 1995c). This device employs a mobile ultramicroelectrode (UME), the

Received for publication 16 April 1997 and in final form 30 July 1997.
Address reprint requests to Dr. P. R. Unwin, Department of Chemistry, University of Warwick, Coventry CV4 7AL, UK. Tel.: 44-1203-523264; Fax: 44-1203-524112; E-mail: p.r.unwin@warwick.ac.uk.

0006-3495/97/11/2771/11 $2.00

response of which provides local information on the topography (Lee et al., 1990; Bard et al., 1991; Kwak and Bard, 1989) and reactivity (Wipf and Bard, 1991; Bard et al., 1991; Pierce et al., 1992; Pierce and Bard, 1993; Macpherson and Unwin, 1994a, b; 1995b, c; 1996) of an interfacial area over which the probe is scanned. The lateral resolution of the SECM, governed primarily by the size of the UME, but also the tip-to-sample separation and interfacial reactivity (Bard et al., 1991), is at the micrometer-to-submicrometer (Fan and Bard, 1996) level.

In the context of the studies reported herein, the previous use of SECM to determine local mass transfer rates through tissues is particularly noteworthy. In initial studies, the primary routes of ionic transport through skin during iontophoresis were investigated and the localized diffusional fluxes of electroactive species, through individual pores in the skin membrane, were measured (Scott et al., 1991, 1993a, b; 1995). Our group has further developed this approach to characterize and quantify local hydrostatically induced convective flow through dentine slices at the level of a single tubule of micrometer dimensions (Macpherson et al., 1995a, b).

In this paper we extend SECM studies of transport in biological systems in two ways. Through studies on laryngeal cartilage, it is first shown that steady-state measurements of the SECM tip current response—as a function of tip/sample separation—provide information on the rate of diffusion of target solutes in the cartilage matrix. This approach is illustrated with studies on the diffusive transport of oxygen and $Ru(NH_3)_6^{3+}$. Second, the use of SECM to quantitatively image osmotically induced convective transport of solutes through soft tissues is illustrated using $Ru(NH_3)_6^{3+}$ as a model probe molecule. To support the experimental studies, SECM mass transport models are formulated to enable UME current data to be related quantitatively to the local flux at the cartilage/solution interface. In the case of imaging experiments, the model allows, for the first time, the lateral variation of mass transport rates across the surface of cartilage to be visualized and compared directly to the corresponding topography.

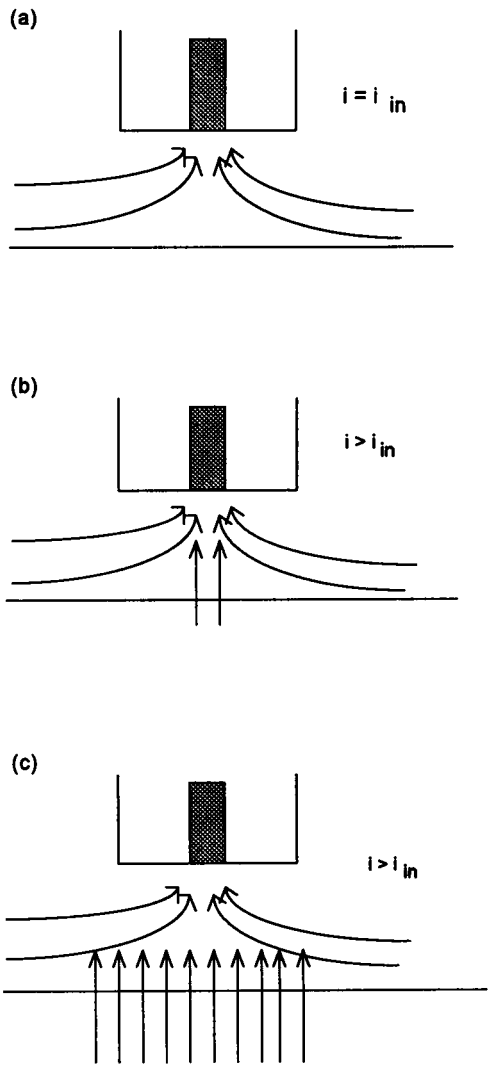

FIGURE 1 Schematic of the limiting transport situations for SECM investigations of induced diffusion and osmotically driven convective flow in tissue. (*a*) When the partition coefficient and/or diffusion coefficient of the target species in the tissue matrix is low, transport to the electrode is mainly by diffusion in the thin gap of solution between the tip and sample surface. (*b*) If the concentration and diffusion coefficient of the species in the sample are of the same order as those in the solution, the electrolysis process serves to induce diffusion in both the solution and biological matrix, enhancing the UME current. (*c*) The UME current is enhanced when there is pressure-driven convection of the solute across the sample, which is manifested as a solute flux at the sample/solution interface.

PRINCIPLES

The response of the SECM, with amperometric probes, is governed by the rate at which a target electroactive solute is transported to the UME during electrolysis. In the studies reported herein, the UME is held at a potential for the transport-limited reduction of an analyte, either $Ru(NH_3)_6^{3+}$ or oxygen. Depending on the type of experiment, the tip is either held at a fixed position or scanned at a distance of a few micrometers above the surface of a thin slice of cartilage. To illustrate the possible factors that could, in principle, affect the UME current, Fig. 1 depicts the available routes for the transport of an analyte, which partitions between an aqueous solution and the cartilage matrix, in the absence and presence of an applied osmotic pressure. Note that under the experimental conditions (see below), contributions to the transport of charged species of interest to the electrode by migration can be neglected.

In the absence of an applied osmotic pressure, the initial conditions are such that there is a dynamic equilibrium of the target species between the solution containing the UME probe and the tissue sample. The simplest scenario is that the electrolytically induced transport of the species of interest to the probe is by simple hindered diffusion in the thin layer of solution between the tip and the sample [Fig. 1 *a*]. In this situation, as the gap between the probe and the

sample decreases, the flux of material to the UME, and hence the steady-state current, falls (Kwak and Bard, 1989). For a given probe geometry, the current depends only on the probe/sample separation and thus variations in current, measured with lateral probe position, can provide topographical information about the surface with a resolution governed primarily by the diameter of the tip electrode (Kwak and Bard, 1989; Bard et al., 1991–1993; Macpherson and Unwin, 1995c).

The above situation will only apply when the concentration and/or diffusion coefficient of the target solute in the solution are much greater than those in the tissue matrix (Barker and Unwin, in preparation). This is because the diffusion-controlled electrolysis process serves to locally deplete the concentration of the solute in the probe/sample gap. The resulting perturbation of the dynamic equilibrium of the solute between the tissue and bathing solution provides the thermodynamic force for the diffusive transport of the solute from the tissue into the solution in the gap between the probe and sample surface [Fig. 1 *b*]. This induced-diffusion situation is similar to the induced-desorption (Unwin and Bard, 1992) and induced-dissolution (Macpherson and Unwin, 1994a, b; 1995a, b; 1996; Slevin et al., 1996) processes studied earlier by SECM. If the diffusive flux of the solute in the tissue sample is of the same order as that in the solution, a measurable contribution to the UME current from diffusion of species in the cartilage matrix is predicted (Barker and Unwin, in preparation).

When the tip UME is scanned over the cartilage sample, with a pressure gradient applied, convective transport of the solute through the cartilage matrix is expected to produce an additional flux at the cartilage/solution interface [Fig. 1 *c*]. This effect serves to increase the current relative to the situation where transport is by hindered and/or induced diffusion. Thus, it should be possible to locate and quantify active areas of fluid flow, with high spatial resolution, by monitoring the differences in the spatially resolved transport-limited current for a target solute, as the tip is scanned over the cartilage surface, in the absence and presence of a pressure gradient. Additionally, by making measurements with electroactive solutes under conditions where the situation in Fig. 1 *a* applies, it should be possible to link local hydraulic permeability or solute diffusivity to the topography of the surface.

MATERIALS AND METHODS

Experimental: materials and solutions

Laryngeal cartilage from pigs approximately six months of age was obtained from the abattoir. The tissue was stored at −20°C until required. It was then stripped of superficial membranes and full depth plugs 5 mm in diameter were punched out with a cork borer. Frozen sections (150 μm) were cut parallel to the surface and, after equilibrating to room temperature in phosphate-buffered saline, mounted in the SECM rig as described below.

After the experiments, some specimens were dehydrated and stained with hematoxylin (cell nuclei), Alcian blue (glycosaminoglycans), and van Gieson's stain (collagen), by standard procedures (Drury and Wallington, 1980).

Hexaammineruthenium(III) chloride (Strem, Royston, UK) was employed at a concentration of 0.01 mol dm^{-3} in aqueous solution for induced-diffusion and osmotic-transport measurements, as well as for the initial stage of partition coefficient measurements. Either 0.2 mol dm^{-3} potassium nitrate (Aldrich, Dorset, UK, 99.999% purity) or 0.2 mol dm^{-3} potassium chloride (Aldrich, AR grade) served as supporting electrolytes; similar results were obtained with each. When the solution also contained polyethylene glycol (PEG; mol wt 15,000–20,000, Aldrich), a level of ~80 g dm^{-3} was employed. Oxygen measurements were made with aerated aqueous 0.1 mol dm^{-3} potassium chloride solution.

Apparatus and instrumentation

The general SECM instrumentation has been described elsewhere (Macpherson et al., 1995a, b; Macpherson and Unwin, 1995a). In contrast to earlier studies, the SECM was equipped with a zoom microscope with video camera and monitor to enable optical viewing of the tip position. The UME tip was a 12.5-μm radius Pt disk electrode, formed by sealing a wire in a glass capillary, which had at the apex a ratio of overall tip radius to active electrode radius of ~10. The UME acted as the working electrode in a conventional two-electrode arrangement, with a silver wire serving as a quasi- reference electrode (AgQRE).

For diffusion measurements, the cartilage sample was mounted on a glass disk (diameter 12.7 mm, thickness 1.6 mm) using a 1:1 volume mixture of nail varnish and "Superglue" (Bostik, Leicester, UK), which was applied sparingly around the circumference of the sample. While setting, which took only several minutes, the cartilage sample was kept moist to prevent any dehydration. The glass disk, with the cartilage surface exposed, was anchored firmly in the base of an SECM cell, so that the surface of the sample was perpendicular to the axis of the UME tip. When an inert surface was required, the glass disk alone was used as the sample.

For hydraulic flow measurements, the cartilage slice was affixed to the end of a glass tube (o.d. 6.00 mm, i.d. 1.60 mm), using the adhesive described above. The tube was then mounted vertically in the base of an SECM cell, as shown schematically in Fig. 2. The setup depicted in Fig. 2 is effectively a two-compartment cell, comprised of solutions in donor and receptor compartments separated by the cartilage slice, with the mobile UME in the receptor solution providing a means of probing transport fluxes with high spatial resolution.

The donor compartment was a variable height reservoir, attached to the end of the glass tube supporting the cartilage sample using poly(tetrafluoroethylene) tubing, as described previously (Macpherson et al., 1995a, b). The position of the reservoir was adjusted to ensure that there was no hydrostatic pressure across the slice during all procedures. As described below, the osmotic pressure across the cartilage sample was controlled by adding solutions containing PEG to the receptor compartment, with an aqueous electrolyte solution of the same ionic strength in the donor compartment, which bathed the cartilage.

Photomicrographs of the cartilage surfaces were taken before and after experiments with an Olympus BH2 microscope.

Procedures

Before measurements, the solution was left in contact with the cartilage sample for up to two hours, with argon bubbled through the solution to effect stirring and de-aerate the solution. For the thin samples employed, this was considered to be sufficient to ensure an equilibrium partitioning of the target solute between cartilage and the aqueous solution, even for cases where the diffusion coefficient in the cartilage matrix was greatly reduced compared to that in aqueous solution. All measurements were made at 298 K.

Approach curves of transport-limited current versus tip/sample separation, above a particular spot on the surface, were obtained by scanning the tip toward the sample surface at a velocity of 2.2 μm s^{-1} from an initial

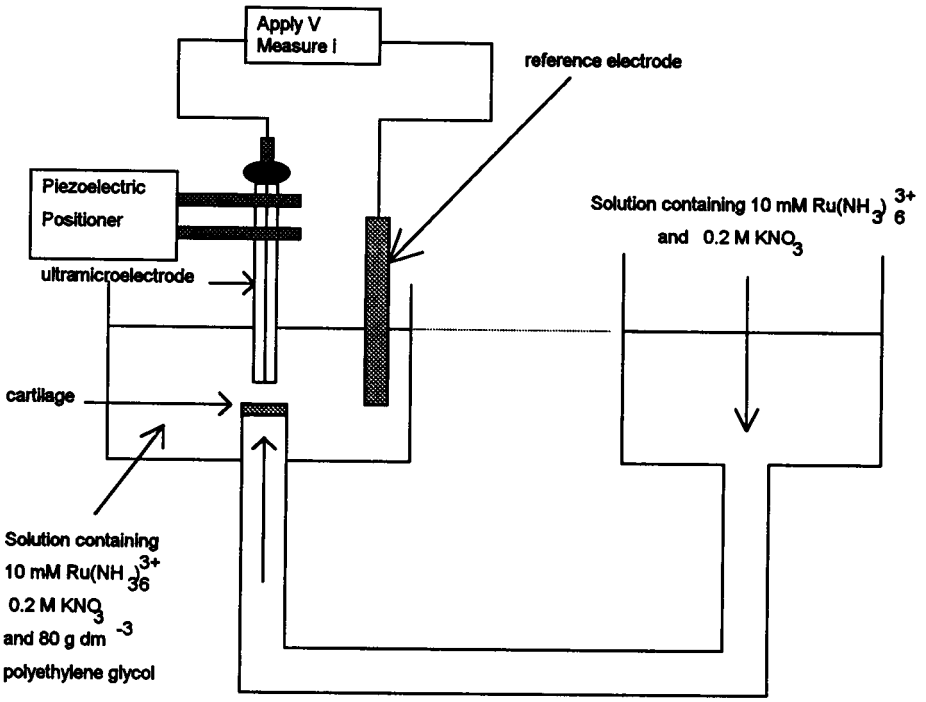

FIGURE 2 Schematic of the SECM arrangement for the study of osmotically driven transport through cartilage.

separation of ~70 μm. The tip potential was held at a value for the transport-limited electrolysis of the target species, and the corresponding current measured as a function of time/position. For measurements of the reduction of $Ru(NH_3)_6^{3+}$ and oxygen (investigated in separate experiments), the potential was held at −0.45 and −0.60 V, respectively, versus AgQRE.

Imaging experiments were carried out exclusively with $Ru(NH_3)_6^{3+}$ as the target species. Data for the transport-limited current for the one-electron reduction of $Ru(NH_3)_6^{3+}$ versus tip position were obtained by scanning the tip at a velocity of 20 μm s^{-1}, in a fixed plane above the cartilage surface. The initial tip/substrate separation, set at the center of images (coordinates $x = 0$ μm, $y = 0$ μm), was typically ~8 μm. In the light of the results from the tip approach measurements, described below, this distance was carefully set by decreasing the UME tip/cartilage separation until the steady-state current, i, was 40% of that measured when the electrode was several millimeters above the cartilage surface (Kwak and Bard, 1989). The current flowing in the latter situation is designated $i(\infty)$.

Initially, the composition of the solution in the two compartments was the same, such that there was no net pressure gradient across the slice, and the steady-state current response for $Ru(NH_3)_6^{3+}$ reduction was due only to hindered (and induced) diffusion. After recording an image in this configuration, an osmotic pressure of 0.75 atm was applied by replacing the receptor solution with one containing PEG at an appropriate concentration (Maroudas and Grushko, 1990).

Changing the composition of the solution in the receptor compartment involved displacing the tip UME from the cartilage surface, typically 500 μm in the normal direction and 1000 μm laterally, draining the cell of solution, and replenishing with the electrolyte solution containing PEG. The ionic strength and concentration of $Ru(NH_3)_6^{3+}$ in the solutions in the donor and receptor compartments was the same (and the activities of the ionic species were expected to be similar). The difference in the activity of water in the two solutions provides the net thermodynamic force for the transport of electrolyte solution across the cartilage sample from the donor to the receptor compartment.

Although PEG, of the molecular weight used, is effectively excluded from cartilage on steric grounds, there are reports of the possible slight ingress of PEG of much lower molecular weight into cartilage over extended periods (Maroudas and Grushko, 1990). By re-scanning the sample within 20–30 min of changing the solution, complications that might arise from the ingress of PEG into the matrix were eliminated. With the instrument employed, the tip could be positioned with bidirectional repeatability at the submicrometer level (Macpherson et al., 1995a, b), enabling the image with osmotic pressure to be recorded over the same area of a sample as that obtained without a pressure.

The procedure for determining, voltammetrically, the partition coefficient of $Ru(NH_3)_6^{3+}$ in cartilage, involved exposing a cartilage slice to 50 cm^3 of bathing solution, with the composition outlined above, for several hours with stirring. After wicking away excess surface fluid from the sample with a lens tissue, the slice was placed in 1.7 cm^3 aqueous desorbing solution containing 0.2 mol dm^{-3} KNO_3. The solution was stirred for several hours before the concentration of $Ru(NH_3)_6^{3+}$ in solution was determined by recording a steady-state linear sweep voltammogram for the reduction process in an Ar-purged solution. The solution volumes employed at each stage ensured that there would be an insignificant depletion of $[Ru(NH_3)_6^{3+}]$ in the bathing solution during the absorption process, while the desorption of labile $Ru(NH_3)_6^{3+}$ from cartilage would essentially go to completion, but yield a voltammetrically measurable solution concentration.

RESULTS AND DISCUSSION

Partition coefficient measurements

The partition coefficient of oxygen has been measured in various cartilaginous materials and has been found to be close to unity, like that of other small neutral species (O'Hare et al., 1991). The partition coefficient of $Ru(NH_3)_6^{3+}$ in the cartilage samples of interest was determined voltammetrically using the procedure outlined above.

Although the SECM measurements of $Ru(NH_3)_6^{3+}$, reported below, were obtained by initially pre-purging the solutions of interest with Ar, this is not an appropriate procedure for handling viable biological tissues. Therefore, an assessment was made of the effect of oxygen on the reduction of $Ru(NH_3)_6^{3+}$, by comparing the linear sweep

voltammetry (LSV) response from aerated and Ar-purged solutions. Fig. 3 shows the typical response recorded in an aerated solution. The shape of the voltammogram is as expected for a reversible process at a UME under steady-state conditions, with the separation between the quarter-wave and three-quarter wave potentials of 58 mV, close to the predicted theoretical value of 56.5 mV (Oldham et al., 1989). Voltammetric measurements after de-aeration of the solution, by outgassing with Ar, resulted in a similar response, indicating that although, in principle, oxygen may be electroactive toward the lower potential range employed, it has a negligible effect on the electrode response with the concentrations of $Ru(NH_3)_6^{3+}$ employed. Thus, in future, use of air-equilibrated media during imaging would not be problematic.

The diffusion coefficient of $Ru(NH_3)_6^{3+}$ may be determined from the magnitude of the diffusion-limited current in Fig. 3. The steady-state diffusion-limited current at a disk UME is given by Saito (1968):

$$i(\infty) = 4naFDc^* \quad (1)$$

where n is the number of electrons transferred per redox event [n = 1 for the reduction of $Ru(NH_3)_6^{3+}$], a is the electrode radius, F is Faraday's constant, and D is the solution diffusion coefficient of the analyte of interest of bulk concentration, c^*. From the data in Fig. 3 $Ru(NH_3)_6^{3+}$, $D = 8.8 \times 10^{-6}$ cm^2 s^{-1}. This value agrees well with that reported by Birkin and Silva-Martinez (1996), for aqueous electrolyte solutions of similar ionic strength.

Voltammetric determination of $Ru(NH_3)_6^{3+}$ following the absorption/desorption procedure described above, in four separate experiments, resulted in voltammograms in the potential region of interest (identified in Fig. 3) with heights of 400–440 pA. Using the value of D for $Ru(NH_3)_6^{3+}$ determined above, these results indicated that the concentration in solution [Eq. 1] was 9.7 ($\pm$0.3) $\times$ 10^{-5} mol dm^{-3}, from which a partition coefficient of $Ru(NH_3)_6^{3+}$ in laryngeal cartilage was calculated as $K_p = [Ru(NH_3)_6^{3+}]_{cartilage}/[Ru(NH_3)_6^{3+}]_{solution} = 3.4$ ($\pm$ 0.1).

SECM tip approach measurements

In the light of the discussion above, tip approach experiments were concerned with determining the extent of SECM-induced diffusion from cartilage to aqueous solution, with each of the two target solutes, oxygen and $Ru(NH_3)_6^{3+}$.

$Ru(NH_3)_6^{3+}$

Typical approach curves for the reduction of $Ru(NH_3)_6^{3+}$ at a tip scanned toward the surface of both a cartilage sample and a glass disk are shown in Fig. 4. The data obtained with both samples are seen to be similar, and in good agreement with the response predicted for an inert surface (Kwak and Bard, 1989). The data indicate that cartilage is a viable sample for high-resolution SECM measurements, in that the tip can approach the surface within a few micrometers.

The results in Fig. 4 clearly indicate that induced desorption of $Ru(NH_3)_6^{3+}$ from the cartilage matrix is a negligible process on the timescale of the SECM measurements. A general SECM model for two-phase diffusion with an arbitrary kinetic barrier at the boundary between the two phases, as applicable to the present studies, has recently been developed (Barker and Unwin, in preparation). Given that $Ru(NH_3)_6^{3+}$ effectively remains in aqueous solution during transfer from the cartilage matrix to the bathing solution, the main resistance to interfacial transfer is likely to be diffusion in the cartilage matrix. With this assumption, and taking account of the partition coefficient measured above, the data in Fig. 4 indicate that the diffusion coefficient of $Ru(NH_3)_6^{3+}$ in cartilage is at least two orders of magnitude lower than in aqueous solution. The implications for SECM

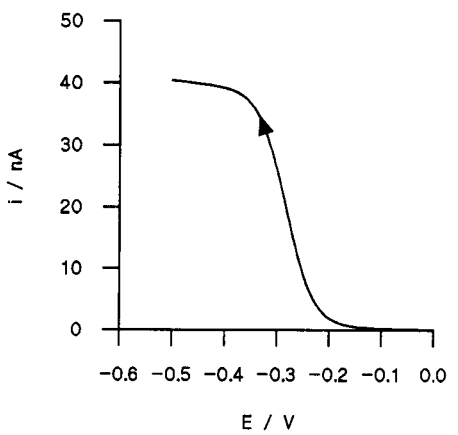

FIGURE 3 Voltammetric response for the reduction of 10 mM $Ru(NH_3)_6^{3+}$ in an aerated solution. The UME potential was scanned from 0.0 V to −0.5 V at a rate of 10 mV s^{-1}.

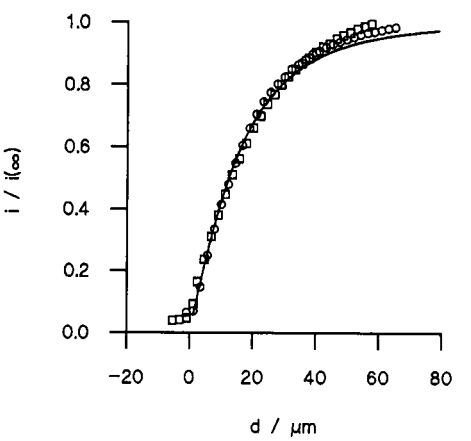

FIGURE 4 Approach curves of normalized current ratio versus tip/substrate separation for the diffusion-controlled reduction of $Ru(NH_3)_6^{3+}$ at a UME tip scanned toward the surface of a flat glass disk (□) and a sample of cartilage (○). The solid line shows the theoretical response (Kwak and Bard, 1989) expected for an inert (impermeable) interface.

imaging measurements are that, in the absence of an applied pressure, SECM current measurements in this system will simply reflect the tip/sample separation.

Although it is well established that for small, low charge density ionic species, the charge on the solute compared to that of the matrix can influence the value of the partition coefficient (Hefferich, 1962; Maroudas, 1968), the effect of charge on the magnitude of the diffusion coefficient was originally thought to be relatively unimportant (Maroudas, 1968; Urban, 1990). It has generally been found that for charged solutes such as Na^+, Cl^-, K^+, SO_4^{2-}, and Li^+, and small neutral species, the diffusion coefficient in cartilage is some 40–60% of that in free solution (Maroudas, 1968, 1975, 1979; Burstein et al., 1993). The measurements reported above, together with other recent studies (Fischer et al., 1995) suggest, however, that for certain small-to-moderate-sized solutes, diffusion coefficients can be significantly reduced compared to the values measured in free solution. For these species, convection is thus likely to be an important transport process (Fischer et al., 1995; Garcia et al., 1996).

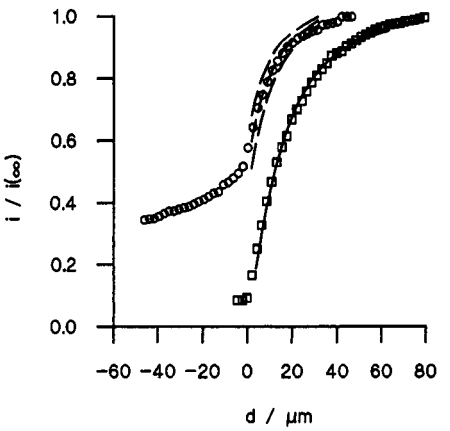

FIGURE 5 Approach curves of normalized current ratio versus tip/substrate separation for the diffusion-controlled reduction of oxygen at an UME tip scanned toward a flat glass surface (□) and a sample of cartilage (○). The solid line shows the theoretical response expected for an inert interface (Kwak and Bard, 1989), while the dashed lines show the theoretical behavior for induced diffusion in the cartilage sample (Barker and Unwin, in preparation) with different values of the diffusion coefficient ratio, $\gamma = 0.6$ (*upper line*), 0.5 (*middle line*), and 0.4 (*lower line*).

Oxygen

The amperometric measurement of oxygen at Pt is potentially complicated by the fact that reduction occurs in two two-electron steps coupled by a fast chemical step (Pletcher and Sotiropoulos, 1993, 1995). The apparent number of electrons transferred in the cathodic reduction of oxygen thus varies from two to four as the mass transport rate decreases from high to lower values. However, steady-state measurements with a 12.5-μm radius UME, as used in this study, have found that the number of electrons transferred in the electrode reaction is close to four (Pletcher and Sotiropoulos, 1993, 1995). Given that the current was found to decrease during the oxygen tip approach measurements reported below, i.e., the mass transfer rate to the tip decreased from that in bulk solution, it is reasonable to assume a four-electron process during such measurements. The assignment of the reduction of oxygen in bulk solution as a four-electron process was further confirmed in that the steady-state current of 9.4 nA measured with the tip far from the surface yielded a diffusion coefficient for oxygen of 2.0×10^{-5} cm^2 s^{-1}, assuming a concentration of 2.5×10^{-4} mol dm^{-3} in air-saturated solution. The diffusion coefficient is in good agreement with that reported elsewhere (Winlove et al., 1984; Pletcher and Sotiropoulos, 1993, 1995).

Typical tip approach curves for both a glass disk and cartilage are shown in Fig. 5. In contrast to the measurements on $Ru(NH_3)_6^{3+}$, there is now a distinct difference in the shapes of the curves with the two different substrates. The behavior observed with the glass surface is in close agreement with the theory for an inert interface, demonstrating that approach measurements involving oxygen reduction can be made. With cartilage as the sample, the current falls off steeply as the tip approaches the cartilage/solution interface (i.e., as d decreases), but there is a characteristic position at which there is a sharp transition to a more gradual decrease in current as the tip is pushed further. The position of the abrupt change in the current gradient was assigned, and confirmed through video microscopy, to be the point at which the tip contacted the cartilage surface ($d = 0$ μm). Thereafter, further movement of the tip serves to compress the cartilage sample, which produces a gradual decrease in the oxygen flux at the UME.

There is considerable interest in understanding the effect of compression on transport in cartilage (Mow et al., 1984; Maroudas et al., 1995); part of the data set in Fig. 5 suggest that UME experiments, of the type described, could provide a simple means for investigating this phenomenon. Note that the results in Fig. 5 (for $d < 0$ μm), together with Eq. 1, indicate that compression of the cartilage produces a decrease in the local analyte concentration and/or diffusion coefficient. More precise information on which of these factors is most important in controlling the lower UME fluxes could be obtained by operating in a chronoamperometric mode, where the diffusion coefficient and concentration of analyte can be determined independently (Winlove et al., 1984; O'Hare et al., 1991).

Assigning the position of zero tip/substrate separation as described above, it is clear that as the tip approaches the cartilage sample, the current for oxygen reduction is enhanced compared to the situation where the target interface is inert. This may be attributed to the electrochemically induced transfer of oxygen from the cartilage matrix to the bathing solution. Assuming a value of unity for the partition coefficient of oxygen between cartilage and aqueous solution, and no kinetic barrier at the cartilage solution/interface, for the reasons outlined above, the data in Fig. 5 (for

$d > 0$ μm) may be analyzed in terms of one unknown variable:

$$\gamma = D'/D \tag{2}$$

where D' is the diffusion coefficient of the analyte in the cartilage matrix. The data in Fig. 5 are in good agreement with calculations of the tip current (Barker and Unwin, in preparation) for $\gamma = 0.5$, suggesting that the diffusion coefficient of oxygen in cartilage is 50% that in aqueous electrolyte. This finding is in good agreement with previous measurements of oxygen diffusion rates in cartilage (O'Hare et al., 1991). Advantages of the present new method over established techniques are: 1) the data used in the diffusion coefficient analysis are obtained without the electrode in contact with the sample, ensuring that the structural integrity of the matrix is maintained; and 2) a targeted region of the surface is probed, opening up considerable scope for spatially resolved diffusion coefficient measurements.

Spatially resolved measurements of interfacial mass transfer at the cartilage/aqueous solution interface

SECM imaging measurements were made on four cartilage samples with similar results, typical of those presented in this section. Fig. 6 *a* shows a normalized diffusion-limited current image for the reduction of $Ru(NH_3)_6^{3+}$ obtained with the donor and receptor solutions of identical composition. In the light of the results of the tip approach measurements above, the UME current in this situation is primarily due to the hindered diffusion of $Ru(NH_3)_6^{3+}$ to the UME, with induced-diffusion as a negligible process. As discussed earlier, under these conditions, the UME current ratio at any point in x-y space can be related to the corresponding tip/sample separation, d. Although an equation defining the relationship between current and tip/substrate separation has been proposed for steady-state conditions (Mirkin et al., 1992), in order to extract topographical information from the data in Fig. 6 *a*, account should be taken of the tip speed.

For a scanning probe moving at a velocity v_{tip} in SECM imaging, the characteristic dimensionless measurement time is given by Macpherson and Unwin (1995a, b):

$$\tau_m = \frac{2D}{v_{tip}a} \tag{3}$$

Under the experimental conditions, $\tau_m = 6.8$. Although, at this measurement time, currents are close to the steady-state values at large tip-substrate separations, hindered diffusion is of a transient nature at closer tip/substrate separations (Bard et al., 1992).

The results of chronoamperometric simulations of the current-distance characteristics for $\tau_m = 6.8$, calculated as outlined elsewhere (Unwin and Bard, 1991; Bard et al., 1992), were found to fit the following empirical relationship

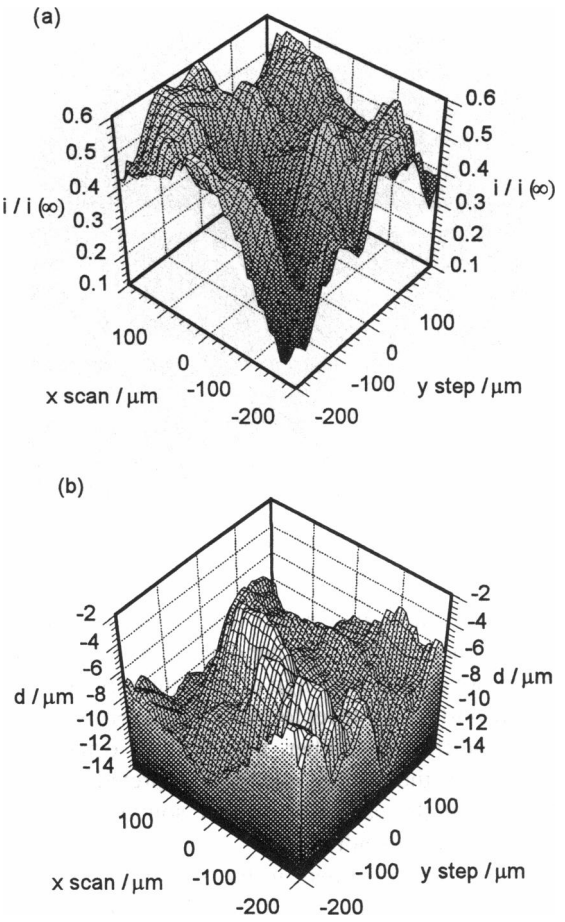

FIGURE 6 (*a*) Normalized diffusion-limited current map for the reduction of $Ru(NH_3)_6^{3+}$ at a tip scanned over a sample of cartilage. (*b*) Corresponding topographical map of the surface after transforming the data in (*a*) using Eq. 4.

over the range of tip substrate distances of interest ($0.2 \leq d/a \leq 0.8$):

$$d/a = 0.9864[i/i(\infty)]^2 + 0.7876[i/i(\infty)] + 0.05320 \tag{4}$$

Although Eq. 4 relates to a tip located above an inert planar surface, it has been suggested that the approach can provide semi-quantitative information on the topography of irregular surfaces (Macpherson and Unwin, 1995b; Macpherson et al., 1995a, b). For the present study, where the aim is to correlate topography and local flux measurements, the use of Eq.4 is considered to be adequate.

Fig. 6 *b* shows the topographical map of the surface that results when the data in Fig. 6 *a* are transformed using Eq. 4. This image reveals the presence of peaks and troughs on the cartilage surface, with characteristic lateral dimensions in the 50–100 μm range and heights of several micrometers. These features are consistent with those seen in optical microscopy (Fig. 7) and correlate with the presence (peaks) and absence (troughs) of cells in the surface layer.

With an osmotic pressure applied across the cartilage sample, there is an additional convective flow of electrolyte solution, from the donor to the receptor compartment. The

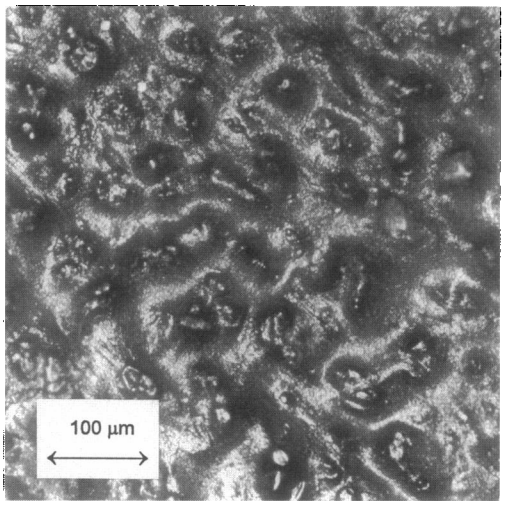

FIGURE 7 Light micrograph of the cartilage surface.

rates of convection anticipated from measurements of the hydraulic conductivities of other connective tissues (Levick, 1987) are not sufficiently high as to require the treatment of mass transport in the receptor solution in terms of coupled convective-diffusion. Rather, the effect of osmotically induced flow in the sample can be interpreted as a flux of $Ru(NH_3)_6^{3+}$ at the cartilage/receptor solution interface, as outlined in the Appendix.

The theoretical treatment in the Appendix demonstrates that topographical effects in the SECM current response, with convective flow in the sample, can be accounted for initially by subtracting the current-space data set obtained with no applied pressure from that measured with the cartilage sample subjected to an applied pressure difference. This procedure assumes that the topography of the sample does not alter under the influence of an applied pressure and that the two measurements are made on the same timescale. Although it has been shown that hydrated cartilage slowly dehydrates when exposed to an aqueous solution containing PEG (Maroudas and Grushko, 1990), which could produce topographical changes in the surface, such effects were considered to be negligible under the SECM conditions for several reasons. First, the exposure time to the PEG solution is much shorter than the 24–48-h period (depending on the thickness of the sample) required for dehydration, and the concentration employed is lower. Second, given the timescale of the dehydration process, one would expect to see time-dependent current images in the PEG solution as the sample morphology changed, and this was not the case. Images recorded sequentially, over a period of 30–45 min, in the PEG bathing solution were found to be essentially the same. The diffusion of PEG into the cartilage matrix, which could cause swelling of the sample, was considered to be negligible under the conditions of the experiments, for the reasons outlined earlier. Indeed, swelling of the sample would be expected to produce current effects opposite to those described below, by decreasing the tip/substrate separation, and hence the current due to hindered diffusion.

Chronoamperometric measurements (Shoup and Szabo, 1982) of $Ru(NH_3)_6^{3+}$ reduction in solutions containing PEG, indicated a decrease in the diffusion coefficient to $D = 6.0 \times 10^{-6}$ cm^2 s^{-1}. Although this shortens the characteristic measurement time (Eq. 4), compared to the situation with no PEG present, calculations showed that the diffusion-limited currents on this timescale were within 2% of those calculated above for the situation without PEG present (in the "worst" case, i.e., at the closest tip/substrate separations) for the range of tip/substrate distances in Fig. 6 *b*. For the greatest tip/substrate separations, the current difference due to timescale effects is ~0.5%. These values are much lower than the current differences observed when the system was under the influence of an osmotic pressure (see below).

Fig. 8 *a*, recorded in the same area as Fig. 6, but with an osmotic pressure difference equivalent to 0.75 atm across the sample, shows the variation of $\Delta i/i(\infty)$ (defined in Eq. A13 in the Appendix) with the tip position in the *x*-*y* plane. This image indicates that there is an increase in the recorded current over most of the area investigated, but that the increases are extremely heterogeneous on a local scale.

The $\Delta i/i(\infty)$ values were converted to corresponding values of interfacial flux using the model outlined in the Appendix. The resulting interfacial mass transport image is

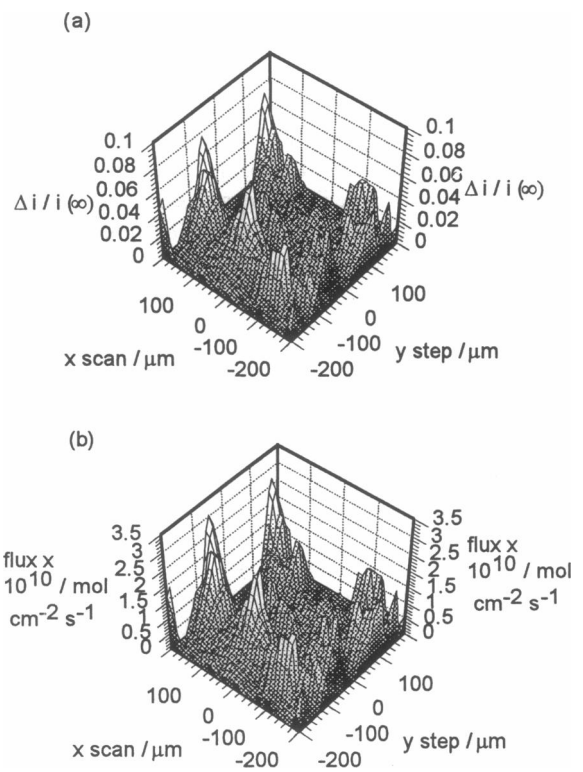

FIGURE 8 (*a*) Normalized current difference map of the same area of cartilage as imaged in Fig. 6, after applying an osmotic pressure across the sample, using the procedure described in the text. (*b*) Corresponding interfacial flux image obtained by transforming the data in (*a*) using Eq. A14.

shown in Fig. 8 *b*. It is clear from this image that there is a wide variation in the interfacial flux over the cartilage with some regions active to fluid flow, while others are not. This represents the first observation that transport across a cartilage sample under an applied pressure is spatially heterogeneous.

By comparing Figs. 6 *b* and 8 *b*, it appears that the active transport areas—such as $x = 200$ μm, $y = -100$ μm; $x = 150$ μm, $y = 150$ μm; and $x = 0$ μm, $y = -100$ μm—correlate with recessed areas. In contrast, the raised topographical areas of the sample—such as the ridge running across the x scan direction between $y = -50$ and $+50$ μm—correlate with inactive or minimal transport pathways. With our assignment of surface recesses and bulges as, respectively, areas where cells are absent and present in the surface layer, the results obtained suggest that fluid follows paths around cells in exiting cartilage, under an applied external pressure.

The spatial variation in observed fluxes could be due to differences in the local fluid velocity and/or solute concentration (Eq. A1), and further experiments will be needed to establish the relative importance of each of these variables. If the partitioning of $Ru(NH_3)_6^{3+}$ into the cartilage matrix is uniform on the scale that can be probed in these experiments, with $K_p = 3.4$, the variations in flux observed suggest that fluid velocities are in the $0-0.08$ μm s^{-1} range.

CONCLUSIONS

SECM has been shown to be a powerful technique for spatially resolved measurements of solute transport in cartilage, with potential applications to many other biological tissues. The newly introduced induced-diffusion method may be used to determine local diffusion rates of solutes in a small volume of tissue without the probe contacting the sample. As a separate approach, the UME response with and without an applied osmotic pressure provides a route to measuring local convective fluxes. Imaging experiments provide a means of correlating local flux measurements with the topography of the sample, allowing maps of the predominant transport pathways to be constructed.

The results obtained indicate—for the first time—that, in laryngeal cartilage, large heterogeneities in transport exist, with the interterritorial region of the ECM providing the most facile transport pathway. Further experiments on viable tissue—which would present no additional technical difficulties—are now planned to assess the physiological significance of this observation.

There is considerable scope for developing the methodology described herein. An attractive feature of amperometric detection is the possibility of making simultaneous or sequential measurements of different solutes in the same tissue sample. Additionally, it should be possible to investigate the effects of changing pressure on mass transport in the same area of a tissue. Although, in these initial experiments, the pressure was generated osmotically to minimize complications from tissue distortion, in specimens where this is not a problem there is no reason why hydrostatic pressure gradients could not be used. It should finally be noted that the techniques described apply to any amperometric electrode, including enzyme-modified amperometric electrodes, opening up the possibility of determining the transport properties of a wide range of model, and physiologically significant, solutes.

APPENDIX

Calculation of the SECM tip current response with osmotic flow

As discussed in the text, when there is no pressure gradient applied across the cartilage slice, transport of $Ru(NH_3)_6^{3+}$ to the tip electrode for electrolysis is principally due to diffusion in the gap between the tip and the tissue surface. The effect of a pressure gradient is to induce an additional convective flow through the tissue sample that produces a flux, $j_{cartilage}$, of $Ru(NH_3)_6^{3+}$ at the cartilage/aqueous interface:

$$j_{cartilage} = -v_z K_p c^* \tag{A1}$$

In Eq. A1, v_z is the velocity of fluid in the cartilage normal to the electrode surface, c^* is the equilibrium analyte concentration in solution, and K_p is the partition coefficient.

The diffusion of $Ru(NH_3)_6^{3+}$ in the axisymmetric cylindrical SECM geometry [see, for example, Fig. 3 in Bard et al. (1992)], under steady-state conditions, is governed by the diffusion equation:

$$D\left(\frac{\partial^2 c}{\partial r^2} + \frac{1}{r}\frac{\partial c}{\partial r} + \frac{\partial^2 c}{\partial z^2}\right) = 0 \tag{A2}$$

where c is the concentration of $Ru(NH_3)_6^{3+}$, and r is the radial coordinate centered on the electrode. The boundary conditions for the problems of interest are:

$$z = 0, \quad 0 \le r \le a \text{ (tip electrode)}: \quad c = 0 \tag{A3}$$

$$z = 0, \quad a < r \le r_s \text{ (glass sheath)}: \quad D\frac{\partial c}{\partial z} = 0 \tag{A4}$$

$$r > r_s, \quad 0 \le z \le d \text{ (radial edge of the tip/substrate domain)}: \quad c = c^* \tag{A5}$$

$$r = 0, \quad 0 < z < d \text{ (axis of symmetry)}: \quad D\frac{\partial c}{\partial r} = 0 \tag{A6}$$

$$z = d, \quad 0 \le r \le r_s \text{ (substrate)}: \quad D\frac{\partial c}{\partial z} = k = -v_z K_p c^* \tag{A7}$$

The term r_s denotes the radial edge of the glass sheath and d denotes the position of the cartilage/solution interface.

The boundary conditions reflect the following facts: 1) $Ru(NH_3)_6^{3+}$ is reduced at the tip at a diffusion-controlled rate; 2) $Ru(NH_3)_6^{3+}$ is inert on the insulating glass sheath surrounding the electrode; 3) $Ru(NH_3)_6^{3+}$ attains its bulk concentration value beyond the radial edge of the tip/substrate domain, which is valid provided that $r_s/a \ge 10$ (Kwak and Bard, 1989); and 4) there is no radial flux at the axis of symmetry. Equation A7 is the restatement of Eq. A1. As with most previous treatments of interfacial processes with SECM, the interface is assumed to be uniformly active.

Even though the aim of SECM mapping is to determine local variations in interfacial reactivity, this is a reasonable initial approach, because the UME response is governed largely by the portion of the interface directly under the tip. In the absence of transport of $Ru(NH_3)_6^{3+}$ in the cartilage (i.e., with no pressure), $k = 0$, and the problem reduces to the case of negative feedback treated originally by Kwak and Bard (1989).

In order to achieve a general solution to the problem, the diffusion equation and boundary conditions are cast into a dimensionless form through the introduction of the following dimensionless parameters:

$$C = c/c^* \tag{A8}$$

$$R = r/a \tag{A9}$$

$$Z = z/a \tag{A10}$$

$$K = ka/Dc^* \tag{A11}$$

The steady-state tip current, i, normalized with respect to the steady-state current when the tip is at an effectively infinite distance from the sample, $i(\infty)$, is:

$$i/i(\infty) = (\pi/2)\int_0^1 (\partial C/\partial Z)_{Z=0} R dR \tag{A12}$$

The problem was solved iteratively using the alternating direction implicit finite difference method, which has been widely employed to solve previous SECM problems (Unwin and Bard, 1991; Pierce et al., 1992). The modifications required for the present problem are straightforward and will not be given in detail.

The concentration throughout the tip/substrate domain was initially set to unity except at the electrode surface, where the concentration was fixed at zero. With $K = 0$ as the condition at the substrate, the current was evaluated until a steady-state value was achieved (Unwin and Bard, 1991; Pierce et al., 1992). The dimensionless rate constant was then incremented, typically in steps of 0.005–0.01, over the range of interest, with the new steady-state current for each rate constant evaluated iteratively.

Fig. 9 shows typical plots of the normalized current ratio, $i/i(\infty)$, as a function of K for several normalized tip/substrate separations. As K increases, the normalized current ratio is seen to increase in a linear fashion, over the range of interest, but the gradient of the slope is clearly dependent on the tip/substrate separation. This effect can be seen more clearly in Fig. 10, which shows the current data in Fig. 9 with the normalized value for

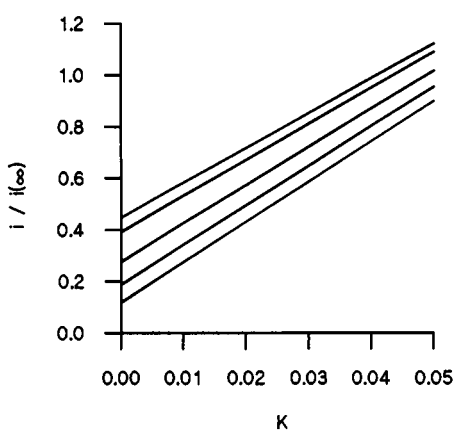

FIGURE 9 Normalized current ratio versus dimensionless rate constant, K, for selected tip substrate positions defined by log $(d/a) = -0.08$ (*upper line*), -0.15, -0.32, -0.5, and -0.7 (*lower line*).

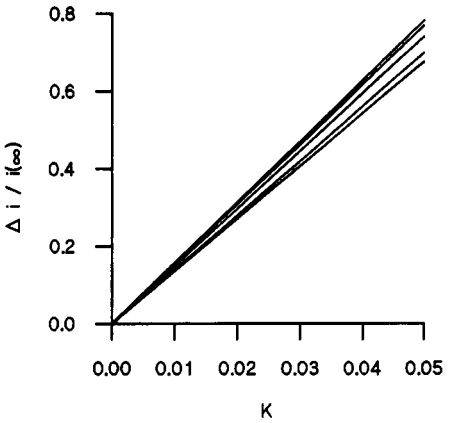

FIGURE 10 Normalized current difference ratio versus dimensionless rate constant, K, for selected tip substrate positions defined by log $(d/a) = -0.7$ (*upper line*), -0.5, -0.32, -0.15, and -0.08 (*lower line*).

$K = 0$, i.e., an impermeable interface, subtracted,

$$\Delta i/i(\infty) = (i_{K>0} - i_{K=0})/i(\infty) \tag{A13}$$

versus K.

The $\Delta i/i(\infty)-K-d/a$ relationship for $0.2 \le d/a \le 1.2$ and $0 \le K \le 5 \times 10^{-2}$ could be described by the following empirical equation:

$$\Delta i/i(\infty) = K[1.464(d/a)^3 - 3.660(d/a)^2 - 0.9457(d/a) + 15.937] \tag{A14}$$

We are grateful to Anna Barker for helpful discussions and for providing a copy of her program for calculating the SECM current response for two-phase diffusion, and R. Ewins for preparing the cartilage samples.

P.R.U. and J.V.M. thank the Engineering and Physical Sciences Research Council for support (GR/K97011).

REFERENCES

Allhands, R. V., P. A. Torzilli, and F. A. Kallfelz. 1984. Measurement of diffusion of uncharged molecules in articular cartilage. *Cornell Vet.* 74:111–123.

Bard, A. J., F.-R. F. Fan, J. Kwak, and O. Lev. 1989. Scanning electrochemical microscopy: introduction and principles. *Anal. Chem.* 61: 132–138.

Bard, A. J., F.-R. F. Fan, and M. V. Mirkin. 1993. Scanning electrochemical microscopy. *In* Electroanalytical Chemistry. Vol. 18. A. J. Bard, editor. Marcel Dekker, New York. 243–373.

Bard, A. J., F.-R. F. Fan, D. T. Pierce, P. R. Unwin, D. O. Wipf, and F. Zhou. 1991. Chemical imaging of surfaces with the scanning electrochemical microscope. *Science.* 254:68–74.

Bard, A. J., P. R. Unwin, D. O. Wipf, and F. Zhou. 1992. Scanning electrochemical microscopy. *Am. Inst. Phys. Conf. Proc.* 241:235–247.

Birkin, P., and S. Silva-Martinez. 1996. A study of the effect of ultrasound on mass transport to a microelectrode. *J. Electroanal. Chem.* 416: 127–138.

Bloebaum, R. D., and A. S. Wilson. 1980. The morphology of the surface of articular cartilage in adult rats. *J. Anat.* 131:333–346.

Burstein, D., M. L. Gray, A. L. Hartman, R. Gipe, and B. D. Foy. 1993. Diffusion of small solutes in cartilage as measured by nuclear magnetic resonance spectroscopy and imaging. *J. Orthop. Res.* 11:465–478.

Drury, R. A. B., and E. A. Wallington. 1980. Carleton's Histological Techniques. Oxford Medical Publications.

Fan, F.-R, and A. J. Bard. 1996. STM on wet insulators: electrochemistry or tunnelling. *Science.* 270:1849–1851.

Fischer, A. E., T. A. Carpenter, J. A. Tyler, and L. D. Hall. 1995. Visualization of mass transport of small organic molecules and metal ions through articular cartilage by magnetic resonance imaging. *Magnet. Res. Imaging.* 13:819–826.

Garcia, A. M., E. H. Frank, P. E. Grimshaw, and A. J. Grodzinsky. 1996. Contributions of fluid convection and electrical migration to transport in cartilage—relevance to loading. *Arch. Biochem. Biophys.* 333:317–325.

Hefferich, F. 1962. Ion Exchange. McGraw-Hill Book Co., Inc., New York.

Jurvelin, J. S., D. J. Müller, M. Wong, D. Studer, A. Engel, and E. B. Hunziker. 1996. Surface and subsurface morphology of bovine humeral articular cartilage as assessed by atomic force microscopy and transmission electron microscopy. *J. Struct. Biol.* 117:45–54.

Kwak, J., and A. J. Bard. 1989. Scanning electrochemical microscopy. Theory of the feedback mode. *Anal. Chem.* 61:1221–1227.

Lee, C., J. Kwak, and A. J. Bard. 1990. Application of scanning electrochemical microscopy to biological samples. *Proc. Natl. Acad. Sci. USA.* 87:1740–1743.

Levick, J. R. 1987. Flow through intestinum and other fibrous matrices. *Q. J. Exp. Physiol.* 72:409–438.

Macpherson, J. V., M. A. Beeston, P. R. Unwin, N. P. Hughes, and D. Littlewood. 1995a. Imaging the action of fluid flow blocking agents on dentinal surfaces using a scanning electrochemical microscope. *Langmuir.* 11:3959–3963.

Macpherson, J. V., M. A. Beeston, P. R. Unwin, N. P. Hughes, and D. Littlewood. 1995b. Scanning electrochemical microscopy as a probe of local fluid flow through porous solids. *J. Chem. Soc. Faraday Trans.* 91:1407–1410.

Macpherson, J. V., and P. R. Unwin. 1994a. A novel approach to the study of dissolution kinetics using the scanning electrochemical microscope: theory and application to copper sulfate pentahydrate dissolution in aqueous sulfuric acid solutions. *J. Phys. Chem.* 98:1704–1713.

Macpherson, J. V., and P. R. Unwin. 1994b. Oscillatory dissolution of an ionic single crystal observed with the scanning electrochemical microscope. *J. Phys. Chem.* 98:11764–11770.

Macpherson, J. V., and P. R. Unwin. 1995a. Scanning electrochemical microscope induced dissolution: rate law and reaction rate imaging for dissolution of the (010) face of potassium ferrocyanide in nonstoichiometric aqueous solutions of the lattice ions. *J. Phys. Chem.* 99: 3338–3351.

Macpherson, J. V., and P. R. Unwin. 1995b. Scanning electrochemical microscopy as a probe of silver chloride dissolution kinetics in aqueous solutions. *J. Phys. Chem.* 99:14824–14831.

Macpherson, J. V., and P. R. Unwin. 1995c. A new look at surface reactions. *Chem. Ind.* 874–879.

Macpherson, J. V., and P. R. Unwin. 1996. Scanning electrochemical microscope-induced dissolution: theory and experiment for silver chloride dissolution kinetics in aqueous solution without supporting electrolyte. *J. Phys. Chem.* 100:19475–19483.

Maroudas, A. 1968. Physiochemical properties of cartilage in the light of ion exchange theory. *Biophys. J.* 8:575–595.

Maroudas, A. 1970. Distribution and diffusion of solutes in articular cartilage. *Biophys. J.* 10:365–379.

Maroudas, A. 1975. Biophysical chemistry of cartilaginous tissues with special reference to solute and fluid transport. *Biorheology.* 12:233–248.

Maroudas, A. 1979. Physiochemical properties of articular cartilage. *In* Articular Cartilage and Osteoarthritis. K. E. Kuettner, R. Scleyerbach, J. G. Peyron, and V. C. Hascall, editors. Raven Press, New York. 355–372.

Maroudas, A., and G. Grushko. 1990. Measurement of swelling pressure of cartilage. *In* Methods in Cartilage Research. A. Maroudas and K. Kuettner, editors. Academic Press, London. 298–301.

Maroudas, A., J. Mizrahi, and E. Benaim. 1995. A study of compressive properties of cartilage using unconfined compression: example of an experimental and theoretical approach. *In* Interstitium, Connective Tissue and Lymphatics. R. K. Reed, N. G. McHale, J. L. Bert, C. P. Winlove, and G. A. Laine, editors. Portland Press. 55–65.

Mirkin, M. V., F.-R. F. Fan, and A. J. Bard. 1992. Scanning electrochemical microscopy. Part 13. Evaluation of the tip shapes of nanometer-size microelectrodes. *J. Electroanal. Chem.* 328:47–62.

Mow, V. C., M. H. Holmes, and W. M. Lai. 1984. Fluid transport and mechanical properties of articular cartilage: a review. *J. Biomech.* 17: 377–394.

O'Hare, D., C. P. Winlove, and K. P. Parker. 1991. Electrochemical method for the direct measurement of oxygen concentration and diffusivity in the intervertebral disk—electrochemical characterization and tissue sensor interaction. *J. Biomed. Eng.* 13:304–312.

Oldham, K. B., J. C. Myland, C. G. Zoski, and A. M. Bond. 1989. Kinetic parameters from steady-state voltammograms at microdisc electrodes. *J. Electroanal. Chem.* 270:79–101.

Pierce, D. T., and A. J. Bard. 1993. Scanning electrochemical microscopy. 23. Reaction localization of artificially patterned and tissue-bound enzymes. *Anal. Chem.* 65:3598–3604.

Pierce, D. T., P. R. Unwin, and A. J. Bard. 1992. Scanning electrochemical microscopy. 17. Studies of enzyme-mediator kinetics for membrane- and surface-immobilized glucose oxidase. *Anal. Chem.* 64:1795–1804.

Pletcher, D., and S. Sotiropoulos. 1993. A study of cathodic oxygen reduction at platinum using microelectrodes. *J. Electroanal. Chem.* 356: 109–119.

Pletcher, D., and S. Sotiropoulos. 1995. Cathodic reduction of oxygen in water and media of low ionic strength. *J. Chem. Soc. Faraday Trans.* 91:457–462.

Saito, Y. 1968. Theoretical study on the diffusion current at the stationary electrodes of circular and narrow band types. *Rev. Polarogr.* 15: 177–187.

Scott, E. R., A. I. Laplaza, H. S. White, and J. B. Phipps. 1993a. Transport of ionic species in skin: contribution of pores to the overall skin conductance. *Pharmacol. Res.* 10:1699–1709.

Scott, E. R., J. B. Phipps, and H. S. White. 1995. Direct imaging of molecular transport through skin. *J. Invest. Dermatol.* 104:142–145.

Scott, E. R., H. S. White, and J. B. Phipps. 1991. Scanning electrochemical microscopy of a porous membrane. *J. Membr. Sci.* 58:71–87.

Scott, E. R., H. S. White, and J. B. Phipps. 1993b. Ionotophoretic transport through porous membranes using scanning electrochemical microscopy: application to in vitro studies of ion fluxes through skin. *Anal. Chem.* 65:1537–1545.

Shoup, D., and A. Szabo. 1982. Chronoamperometric current at finite disk electrodes. *J. Electroanal. Chem.* 140:237–245.

Slevin, C. J., P. R. Unwin, J. A. Umbers, and J. A. Atherton. 1996. A new approach to the measurement of transfer rates across immiscible liquid/liquid interfaces. *J. Chem. Soc. Faraday Trans.* 92:5177–5180.

Torzilli, P. A., T. C. Adams, and R. J. Mis. 1987. Transient solute diffusion in articular cartilage. *J. Biomech.* 20:203–214.

Unwin, P. R., and A. J. Bard. 1991. Scanning electrochemical microscopy. 9. Theory and application of the feedback mode to the measurement of following chemical reaction rates in electrode processes. *J. Phys. Chem.* 95:7814–7824.

Unwin, P. R., and A. J. Bard. 1992. Scanning electrochemical microscopy. 14. Scanning electrochemical microscope induced desorption: a new technique for the measurement of adsorption/desorption kinetics and surface diffusion rates at the solid/liquid interface. *J. Phys. Chem.* 96: 5035–5045.

Urban, J. P. G. 1990. Solute transport between tissue and environment. *In* Methods in Cartilage Research. A. Maroudas and K. Kuettner, editors. Academic Press, London. 241–248.

Winlove, C. P., K. H. Parker, and R. C. Oxenham. 1984. The measurement of oxygen diffusivity and concentration by chronoamperometry using microelectrodes. *J. Electroanal. Chem.* 170:293–304.

Wipf, D. O., and A. J. Bard. 1991. Scanning electrochemical microscopy. 10. High resolution imaging of active sites on an electrode surface. *J. Electrochem. Soc.* 138:L4–L6.